Recent very hot summers in northern hemispheric land areas measured by wet bulb globe temperature will be the norm within 20 years

Chao Li, Xuebin Zhang, Francis W. Zwiers, Yuanyuan Fang & Anna M. Michalak

2017

Original citation:

Li, C., Zhang, X., Zwiers, F. W., Fang, Y., & Michalak, A. M. (2017). Recent very hot summers in northern hemispheric land areas measured by wet bulb globe temperature will be the norm within 20 years. *Earth's Future, 5*(12), 1203–1216. https://doi.org/10.1002/2017EF000639

AGU PUBLICATIONS

Earth's Future

RESEARCH ARTICLE
10.1002/2017EF000639

Special Section:
Avoiding Disasters: Strengthening Societal Resilience to Natural Hazards

Recent Very Hot Summers in Northern Hemispheric Land Areas Measured by Wet Bulb Globe Temperature Will Be the Norm Within 20 Years

Chao Li[1,2], Xuebin Zhang[3], Francis Zwiers[1], Yuanyuan Fang[2], and Anna M. Michalak[2]

[1]Pacific Climate Impacts Consortium, University of Victoria, Victoria, BC, Canada, [2]Department of Global Ecology, Carnegie Institution for Science, Stanford, CA, USA, [3]Climate Data and Analysis Section, Climate Research Division, Environment and Climate Change Canada, Toronto, ON, Canada

Abstract Wet bulb globe temperature (WBGT) accounts for the effect of environmental temperature and humidity on thermal comfort, and can be directly related to the ability of the human body to dissipate excess metabolic heat and thus avoid heat stress. Using WBGT as a measure of environmental conditions conducive to heat stress, we show that anthropogenic influence has very substantially increased the likelihood of extreme high summer mean WBGT in northern hemispheric land areas relative to the climate that would have prevailed in the absence of anthropogenic forcing. We estimate that the likelihood of summer mean WGBT exceeding the observed historical record value has increased by a factor of at least 70 at regional scales due to anthropogenic influence on the climate. We further estimate that, in most northern hemispheric regions, these changes in the likelihood of extreme summer mean WBGT are roughly an order of magnitude larger than the corresponding changes in the likelihood of extreme hot summers as simply measured by surface air temperature. Projections of future summer mean WBGT under the RCP8.5 emissions scenario that are constrained by observations indicate that by 2030s at least 50% of the summers will have mean WBGT higher than the observed historical record value in all the analyzed regions, and that this frequency of occurrence will increase to 95% by mid-century.

Key Points:
- Human influence has increased summer wet bulb globe temperature (WBGT)
- Summer WBGT greater than the 1973–2012 record is now at least 70 times as likely
- The 1973–2013 summer WBGT records will be the norm within 20 years

Supporting Information:
- Supporting Information S1

Correspondence to:
Chao Li, chaoli@uvic.ca

Citation:
C, Li., Zhang, X., Zwiers, F., Fang, Y., & Michalak, A. (2017). Recent Very Hot Summers in Northern Hemispheric Land Areas Measured by Wet Bulb Globe Temperature Will Be the Norm Within 20 Years. *Earth's Future*, *5*, 1203–1216, http://doi:10.1002/2017EF000639

Received 9 JUL 2017
Accepted 13 OCT 2017
Accepted article online 17 OCT 2017
Published online 12 DEC 2017

1. Introduction

It is now well recognized that the likelihood of extreme hot summers has significantly increased due to anthropogenically induced warming. Stott et al. (2004) showed that human influence had more than doubled the likelihood of the extremely hot European summer of 2003 at the time, and human influence has further increased the likelihood after 10 years with additional warming (Christidis et al., 2014). Sun et al. (2014) estimated that anthropogenic influence has increased the likelihood of the historically hot summer of 2013 in Eastern China to more than 60 times its preindustrial level. Building on Sun et al. (2014) and Mueller et al. (2016) systematically examined the occurrence of record hot summers since 1950 in many land regions. They found that human influence has made record high summer temperature at least 10 times as likely and projected that the historically hottest summers would become the norm for more than half of the world's population within 20 years.

Summer mean air temperature can be an important indicator of environmental conditions conducive to heat stress. Sun et al. (2014) showed that higher summer temperatures are directly connected to a greater number of heatwave days defined as daily maximum temperature greater than 35°C and an earlier start and later end of heatwave seasons in Eastern China. Air temperature alone is not necessarily the best indicator of environmental conditions conducive to heat stress on human health, however. Humans maintain a body core temperature near 37°C through convection, conduction, radiation, and evaporation. A human body core temperature above 39°C will create health risks (Parsons, 2003). Hot temperatures with high humidity reduce the ability of the human body to dissipate metabolic heat, leading to increased body core temperature. It is therefore the combination of heat and humidity that really matters (Sherwood & Huber, 2010). Wet bulb globe temperature (WBGT), an indicator that takes temperature and humidity into account, is often used in the management of physical human workloads in direct sunlight, such as endured by athletes, outside workers, and military personnel.

To determine whether anthropogenic influence has had a detectable impact on environmental conditions conducive to heat stress, Knutson and Ploshay (2016) compared observed trends in global and regional mean summer WBGT since 1973 with those simulated by climate models. They found that the observed trends are consistent with model simulations only if anthropogenic forcing is included. Nevertheless, a rigorous statistical comparison of models and observations (e.g., a "fingerprint" analysis) is still needed to reinforce our confidence in the complex causes of WBGT change. WBGT and its variants have also been used to project future changes in heat stress environmental conditions (e.g., Diffenabugh et al., 2007; Dunne et al., 2013; Fisher & Knutti, 2012; Pal & Eltahir, 2015; Willet & Sherwood, 2012; Zhao et al., 2015). Most of these studies rely primarily on simulations with little reference to observations, due primarily to the paucity of homogenous long-term humidity records. As climate models tend to underestimate typical heat stress indices (e.g., WBGT) over many parts of the world such as in the humid tropics and subtropics (Zhao et al., 2015), projections of heat stress indices constrained by past observations would potentially be more reliable for future adaptation planning. The recently compiled HadISDH observational records for surface humidity and temperature (Willett et al., 2014) enable us to disentangle the complex causes of WBGT change through a statistically rigorous "fingerprint" analysis, and to explore future WBGT change constrained by observations.

Here, using the rigorous "fingerprint" method and HadISDH observational records for surface humidity and temperature, we first examine whether anthropogenic influence is detectable in the historical summer WBGT changes by comparing the evolution of WBGT in the observations and in model simulations under different external forcings over northern hemispheric land areas with sufficient observations. We then assess the extent to which anthropogenic influence has altered the likelihood of record high summer WBGT during 1973–2012 in different land regions. Results from the "fingerprint" detection analysis are used to constrain projections of the future as observation-constrained projections give us better confidence compared to native model projections (e.g., Allen et al., 2000; Stott & Kettleborough, 2002).

2. Materials and Methods

2.1. Wet Bulb Globe Temperature

Among the various heat stress indictors (Buzan et al., 2015), WBGT is the ISO standard for quantifying human thermal comfort (ISO, 1989). It has well validated thresholds that relate directly to levels of industrial and military labor capacity (Willet & Sherwood, 2012). For example, the U.S. military recommends a cycle of 30 min work and 30 min rest for heat-acclimated individuals to conduct heavy labor (350–500 kcal/h) under an environment with WBGT between 31.1 and 32.2°C (88–90°F). Different methods have been used to compute WBGT (Lemke & Kjellstrom, 2012). Two general types of WBGT have been calculated to respectively represent outdoor and indoor conditions. WBGT for indoor conditions involves the use of dry bulb air temperature as well as humidity. The calculation of outdoor WBGT additionally involves the use of wind and some measure of direct sunlight exposure. Due to the lack of reliable wind and sunlight data, we compute WBGT (°C) as a weighted sum of wet bulb temperature (WBT, °C) and air temperature (TA, °C) such that $\mathrm{WBGT} = 0.7 \times \mathrm{WBT} + 0.3 \times \mathrm{TA}$ (Liljegren et al., 2008). The resulting temperature represents a lower limit for WBGT in well shaded or indoor conditions, similar to that studied by Dunne et al. (2013) and Knutson and Ploshay (2016). We compute WBT (and thus WBGT) based on TA and relative humidity (RH) following the method of Stull (2011). This method has been shown to be reliable for TA between −20 and 50°C and for 5–100% RH.

2.2. Observational Data and Climate Model Output

We use observed monthly mean surface TA and RH for 1973–2012 from the recently compiled HadISDH 2.0.1.2015p 5° × 5° gridded dataset (Willett et al., 2014). We use simulated monthly mean surface TA and RH from climate models participating in the Coupled Model Intercomparison Project Phase 5 (CMIP5) to estimate climate responses to external forcing and natural internal variability. Simulations from a particular model are selected if there are at least three ensemble members under the same external forcing and if historical simulations are either available or can be extended to the year 2012. These include 78 simulations from 14 models with historical variations in all forcing agents (ALL), including greenhouse gases, aerosol, ozone, land cover, and natural external forcing, 30 simulations from 6 models with historical greenhouse-gas changes (GHG), and 42 simulations from 7 models with historical natural forcing only (NAT). Many CMIP5

ALL simulations end in the year 2005. We extend them to 2012 with either extended ALL simulations from the historicalExt experiment, or if not available the corresponding projections under the RCP8.5 emissions scenario (Representative Concentration Pathway emissions scenario) with approximate total radiative forcing in 2100 relative to 1750 of 8.5 W m^{-2}. The use of other RCPs for data extension makes little difference because radiative forcing differs negligibly between RCPs over the period 2006–2012 (Intergovernmental Panel on Climate Change [IPCC], 2013). We also use over 18,000 model-years of preindustrial control simulations from 35 models for estimating internal variability. Projection of future heat stress is based on 49 RCP8.5 simulations from 12 climate models. See Table S1, Supporting information for details on the climate models and simulations.

2.3. Data Processing

We calculate the observation-based estimates of summer WBGT by averaging monthly values over three summer months if all monthly values are available; the estimate is marked as missing otherwise. Limited data availability restricts our analysis to the region between 10 and 60°N (Figure 1). As such, the three summer months are June, July, and August. Summer WBGT anomalies relative to a 30-year baseline period 1973–2002 are then calculated for grid cells with 27 or more years of data during the baseline period, and are otherwise flagged as missing. Grid cells with at least 36 years of anomalies data during 1973–2012 are analyzed.

We compute monthly values of WBGT with monthly TA and RH on the native grids of the models to preserve internal consistency between TA and RH. These WBGT data are then regridded to the 5° × 5° HadISDH grid using the four nearest grid cell values and inverse distance weighting. Model ocean grid cells are excluded from the interpolation. The regridded ALL, GHG, and NAT simulations are masked (set to missing) to mimic the availability of observations. We divide preindustrial control simulations into 474 nonoverlapping 40-year segments to match the 1973–2012 historical period, and then similarly interpolate and mask each segment. Summer WBGT anomalies relative to 1973–2002 are then calculated for all simulations in the same way as for the observations.

We consider changes of summer WBGT in 10 SREX land regions (Seneviratne et al., 2012) between 10 and 60°N with sufficient observations (Figure 2a). These regions include WNA (West North America), CNA (Central North America), ENA (East North America), NEU (North Europe), MED (Mediterranean), NAS (North Asia), CAS (Central Asia), TIB (Tibetan Plateau), EAS (East Asia), and SAS (South Asia).

2.4. The Optimal Detection Methodology

We compare observed and modeled summer WBGT using the total least squares based optimal fingerprinting method (Allen & Stott, 2003) as implemented by Ribes et al. (2013). The method represents the observations as follows:

$$\mathbf{Y}^* = \mathbf{X}^* \times \boldsymbol{\beta}$$

$$\mathbf{Y} = \mathbf{Y}^* + \varepsilon_{\mathbf{Y}}$$

$$\mathbf{X} = \mathbf{X}^* + \varepsilon_{\mathbf{X}}$$

where $\mathbf{Y}$ is the vector of observations whose elements are the 5-year mean summer WBGT anomalies of different spatial regions (as will be further explained); $\mathbf{Y}^*$ is the climate response to all external forcings; $\varepsilon_{\mathbf{Y}}$ represents the unforced internal variability in the observations; $\mathbf{X}^*$ is the matrix of true but unknown modeled responses to different external forcings, with each column corresponding to the response to a particular forcing; $\mathbf{X}$ is the matrix of estimates of modeled responses to different external forcings based on the available simulations; $\varepsilon_{\mathbf{X}}$ represent the effects of internal variability on the estimates of modeled responses that cannot be averaged out due to limited ensemble size; $\boldsymbol{\beta}$ is the vector of scaling factors to be estimated. The estimates of modeled responses are multi-model ensemble means. The optimal analysis requires two independent estimates of the covariance matrix of the internal variability, which are obtained using a regularized

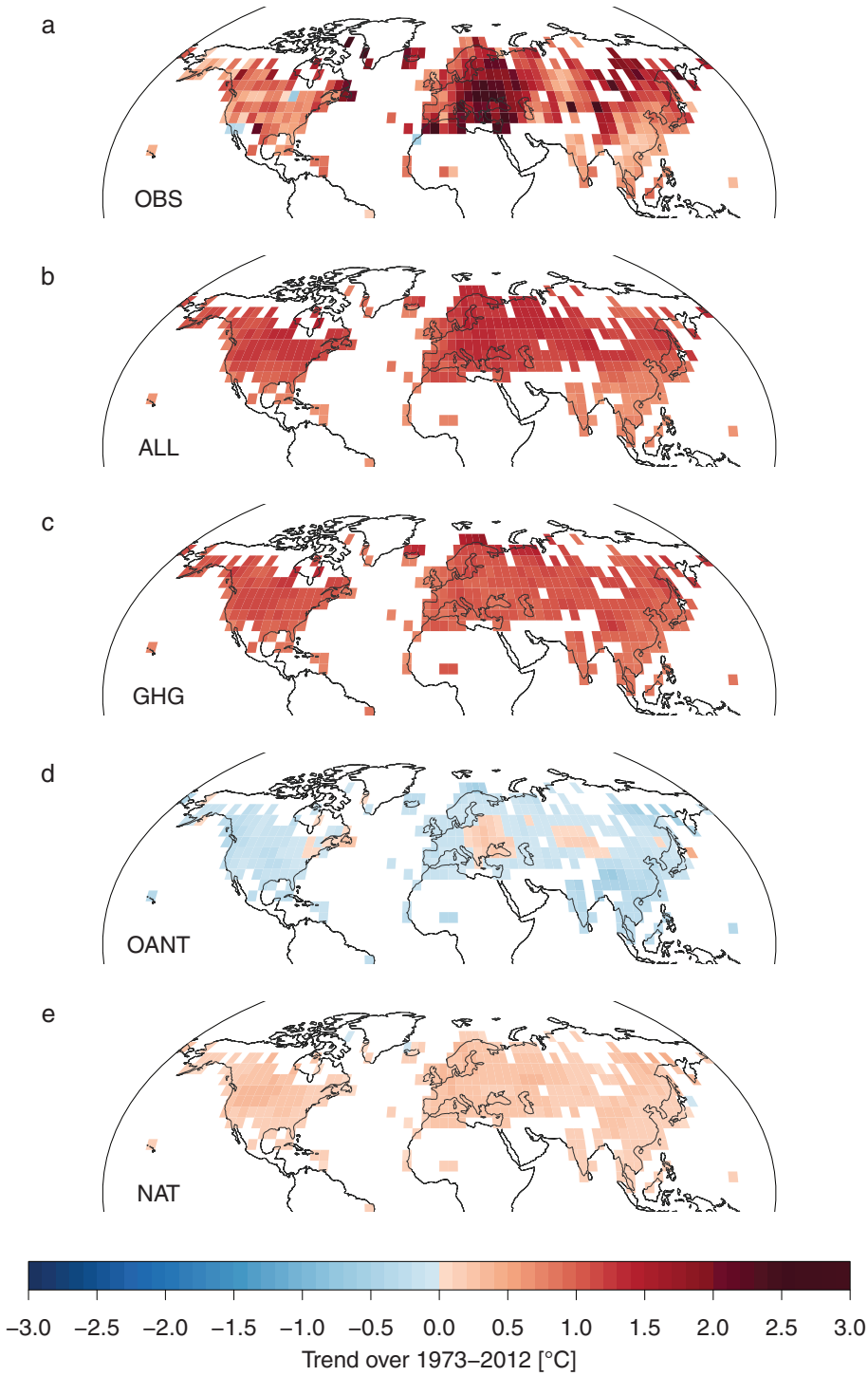

Figure 1. Summer wet bulb globe temperature (WBGT) has increased during 1973–2012. Panels show the 1973–2012 trends (°C) in summer (Jun–Jul–Aug) WBGT for HadISDH observations (a), for CMIP5 model responses to ALL (b), GHG (c), OANT (d), and NAT (e). Regions without sufficient observations are marked as white. ALL, GHG, OANT, and NAT denote respectively to modeled responses to historical natural and anthropogenic forcings, historical greenhouse-gas changes, historical anthropogenic forcings other than greenhouse gases, and historical natural forcings. Modeled responses to ALL, GHG, and NAT are estimated as the multi-model ensemble means of the corresponding native model simulations. The model simulated OANT response is estimated by subtracting the sum of responses to GHG and NAT from ALL.

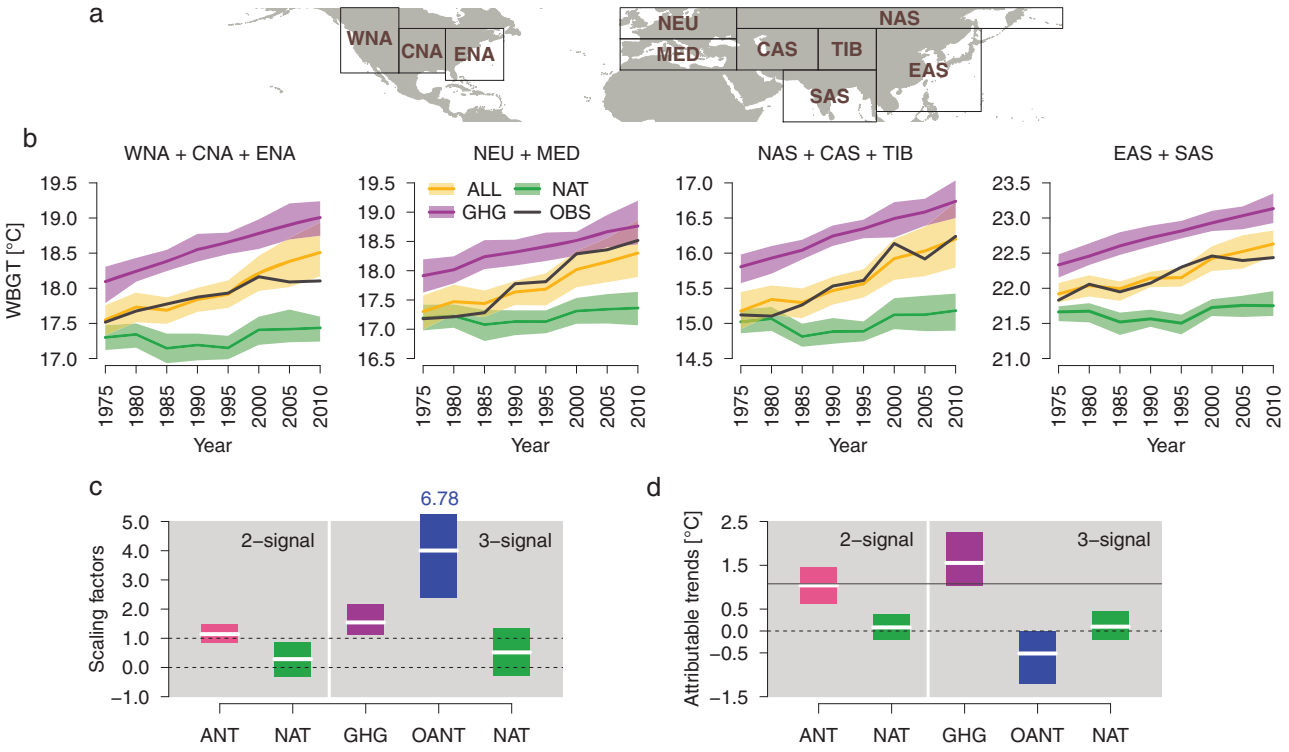

Figure 2. The observed increase of summer wet bulb globe temperature (WBGT) can be reproduced only when anthropogenic forcing is included. (a) Geographic boundaries of the 10 SREX regions between 10 and 60° N (WNA, Western North America; CAN, Central North America; ENA, Eastern North America; NEU, Northern Europe; MED, Mediterranean Basin; NAS, North Asia; CAS, Central Asia; TIB, Tibet; SAS, South Asia; EAS, East Asia). (b) Observed and simulated 5-year mean summer WBGT. To plot this figure, we reconstituted full WBGT values from the observed and simulated anomalies. We added the observed 1973–2002 summer WBGT climatology to the observed anomalies to obtain the full observed summer WBGT values, added the observed climatology to the model-simulated anomalies under ALL forcings to obtain climatologically-bias-adjusted summer WBGT values under ALL, added the observed climatology minus the modeled climatological difference between ALL and NAT to the NAT anomalies to obtain climatologically bias-adjusted values under NAT, and added the observed climatology minus the modeled climatological difference between ALL and GHG to the GHG anomalies to obtain climatologically-bias-adjusted values under GHG. Solid lines show the time series for HadISDH observations (black), adjusted CMIP5 model responses to ALL (yellow), GHG (purple), and NAT (green) forcings. Shaded bands represent the 5–95% uncertainty ranges of the corresponding adjusted simulations. (c) Best estimates of scaling factors (white horizontal lines) and their 5–95% uncertainty ranges (bars) for the global spatiotemporal fingerprint analyses. (d) The observed trend in land average summer WBGT (solid black line), and the best estimates (white horizontal lines) and 5–95% ranges (bars) of the attributable trends to ANT (pink) and NAT (green) from the 2-signal analysis, and to GHG (purple), OANT (blue) and NAT (green) from a three-signal analysis.

estimator (Ribes et al., 2013) from both preindustrial control simulations and interensemble differences of historical simulations (see Supporting Information).

Detection of the influence of a particular external forcing agent while accounting for the influence of other external forcings enhances our confidence in detection and attribution. To this end, we conduct a two-signal analysis that uses ALL and NAT responses as predictors in the regression to derive scaling factors for anthropogenic forcing (ANT) and NAT. We also conduct a three-signal analysis in which ALL, GHG, and NAT responses are predictors in the regression to derive scaling factors for GHG, other anthropogenic forcing agents consisting of aerosols, ozone, and land use change (OANT), and NAT. The online supporting information provides details for the derivation of the relevant scaling factors.

Our analyses are conducted on space–time series of summer WBGT consisting of four spatial dimensions and 8 – 1 = 7 temporal dimensions. That is the observations vector **Y** has $4 \times 7 = 28$ dimensions. The 8 – 1 = 7 temporal dimensions correspond to nonoverlapping 5-year means of regional anomalies during 1973–2012 relative to the 1973–2002 baseline period (one temporal degree of freedom is lost in each region because all data involved in the regression analysis are expressed as anomalies). The four spatial dimensions are represented by area weighted averages over four continental regions, with North America consisting of WNA, CNA, and ENA regions, Europe consisting of NEU and MED regions, Northwest Asia consisting of NAS, CAS, and TIB regions, and Southeast Asia consisting of EAS and SAS regions. We also implemented the analyses on space–time series of WBGT consisting of 10 spatial dimensions corresponding to the 10 SREX regions and the same 7 temporal periods (i.e., vector **Y** has $10 \times 7 = 70$ elements). Note

that all else being equal, a smaller spatiotemporal dimension is preferred because covariance matrix estimation uncertainty is reduced. We obtained qualitatively similar results for the 4 and 10 spatial dimension cases (Figure S1).

The scaling factors and their confidence intervals are used to infer whether the modeled responses to external forcings are detectable in the observations and whether the modeled responses are consistent with the observations. A scaling factor with a 90% uncertainty range above zero indicates the detection of the corresponding response in the observations at the 5% significance level. If the confidence interval also includes one, the modeled response is considered to be consistent with the observations. Reliable attribution of observed changes to particular forcings also requires that other competing explanations have been eliminated, that model simulated variability is comparable to those in the observations, and that the mechanisms leading to the changes are understood. As our analyses are based on modeled responses to the most important known external forcings, we use the regression analyses to estimate attributable warming.

2.5. Long-Term Trend Attribution

Trends along with their 90% confidence intervals are estimated using the nonparametric Sen's slope estimator (Sen, 1968). Warming attributable to external forcings is estimated based on the detection results. Choices have to be made when estimating attributable warming at regional scales. These include a choice between the use of results from regional detection analysis for individual regions (e.g., Christidis et al., 2014; Mueller et al., 2016; Stott et al., 2004; Sun et al., 2014), or from a global detection analysis that includes individual regions (e.g. Christidis et al., 2010, 2012) as well as choice about the way in which the detection results are used when computing attributable warming and the associated confidence interval. Estimation based on regional analysis has the advantage of fitting the modeled responses to observations for individual regions, but it also has the disadvantage of having larger uncertainty in regional detection due to the reduced signal-to-noise ratio at regional scales. Estimation based on a spatiotemporal global analysis may be a better compromise between the reduction in regional details and the increase of internal variability at the regional scale. In this study, we estimate attributable warming based on detection results of such a global analysis. While the widely used method of estimating attributable warming is to first compute the linear trends in the modeled responses and then multiply the trends by the corresponding scaling factors and their confidence intervals, here we use observation-constrained reconstructions to estimate attributable warming, based on the method of Christidis et al. (2010).

Our method for calculating attributable trends and the uncertainties involves the following steps:

(i) Noise-contaminated responses. To consider internal variability in the modeled responses, we produce multiple realizations of noise-contaminated responses by adding a sample of noise to the modeled responses to ANT or NAT forcing. Noise is obtained by scaling the 40-year segments of preindustrial control simulations by $1/\sqrt{ne}$, where ne is the effective ensemble size used in estimating the modeled responses. For the NAT response, the effective ensemble size ne_{NAT} is $N^2/\left(\sum_{i=1}^{N} 1/N_i\right)$, where N is the number of climate models and N_i is the number of ensemble members for model i. The ANT response is estimated as the difference between ALL and NAT responses, and thus, the effective ensemble size for ANT ne_{ANT} is $ne_{\mathrm{ALL}}ne_{\mathrm{NAT}}/(ne_{\mathrm{ALL}}+ne_{\mathrm{NAT}})$, where ne_{ALL} and ne_{NAT} are respectively the effective ensemble sizes in estimating the ALL and NAT responses. As there are 474 segments of preindustrial control simulations available, we can produce 474 samples of the responses to either ANT or NAT forcing with an internal variability component that reflects the variation in multi-model responses that would be expected in independent replications.

(ii) Observation-constrained reconstructions. We generate a sample of 500 plausible estimates of each scaling factor for, for example, the two-signal analysis (see the Supporting information for the generation procedure). We then apply each estimate of the scaling factors to the 474 samples of noise-contaminated responses, producing 474 realizations of observation-constrained responses to either ANT or NAT forcing. Observation-constrained responses to ALL are obtained by adding the observation-constrained ANT and NAT responses. These 474 observation-constrained responses to ANT, NAT, or ALL are then added respectively to the 474 40-year segments of preindustrial control simulations to produce 474 samples of observation-constrained reconstructions of 5-year mean anomalies of summer WBGT during 1973–2012 under the corresponding forcing. Repeating the process across the 500 estimates of scaling factors, we obtain 500×474 samples of

observation-constrained reconstructions under ANT, NAT, and ALL forcing. Observation-constrained reconstructions under GHG, and OANT are obtained similarly based on a three-signal analysis.

(iii) Attributable warming and its confidence interval. We use the Sen's slope estimator (Sen, 1968) to estimate a trend from each of the 500 × 474 samples of observation-constrained reconstructions of 5-year mean anomalies of summer WBGT for each forcing. The median and 90% ranges of these trends are used to represent the best estimate and the 90% confidence interval of attributable warming.

2.6. Event Attribution for Record WBGT

The summer with the highest mean WBGT during 1973–2012 is defined as the record hot summer and the corresponding summer mean WBGT as the record WBGT. Table S2 lists the year of occurrence of the record hot summer and the associated record WBGT value for the entire land area and for individual SREX regions. We define $P_{(1975,\,NAT)}$ as the probability for WBGT to be at least as large as the record WBGT in the climate around the year 1975 (represented by 1973–1977) in the naturally forced world, and $P_{(1975,\,ALL)}$ and $P_{(2010,\,ALL)}$ as the corresponding probabilities in the climates around 1975 ($P_{(1975,\,ALL)}$) and around 2010 (represented by 2008–2012; $P_{(2010,\,ALL)}$) in the world that is influenced by both natural and anthropogenic forcings. We define three risk ratios to assess anthropogenic influence on the occurrence of the record WBGT:

$$RR_1 = P_{(1975,ALL)}/P_{(1975,NAT)}$$

$$RR_2 = P_{(2010,ALL)}/P_{(1975,ALL)}$$

$$RR_3 = P_{(2010,ALL)}/P_{(1975,NAT)}$$

These risk ratios quantify how many times as likely the occurrence of the record WBGT is under one climate scenario compared to under another. In particular, RR_1 reflects the impact of anthropogenic influence as of the year around 1975; RR_2 reflects the further impact of changes in external forcing up to the year around 2010, which is expected to be mainly anthropogenic in origin; RR_3 measures the total impact of anthropogenic influence relative to the naturally forced world, assuming only minor differences due to the impact of natural forcing between the year around 1975 (represented by 1973–1977) and the year around 2010 (represented by 2008–2012). We estimate the probabilities and thus the risk ratios as follows.

From step (ii) in Section 'Long-Term Trend Attribution', we have obtained 500 × 474 samples of observation-constrained reconstructions of 5-year mean anomalies of summer WBGT under NAT or ALL forcing, each consisting of eight values corresponding to the eight nonoverlapping 5-year mean anomalies during 1973–2012. We use the first and last data values to represent respectively the expected summer WBGT anomalies around the years 1975 and 2010 under the relevant forcing. To represent the year-to-year variability in the three epochs (1973–1977 under NAT, 1973–1977 under ALL, and 2008–2012 under ALL), the first data value in each of the reconstructions under NAT, the first under ALL and the last under ALL are then added respectively to the 474 40-year segments of control simulations of annual summer WBGT anomalies, resulting in samples of 474 × 40 plausible annual anomalies in these three epochs. We transform the resulted anomalies to absolute summer WBGT values by adding the observed 1973–2002 WBGT climatology to the anomalies under ALL, and adding the observed climatology minus the modeled climatological difference between ALL and NAT to the anomalies under NAT. Empirical probabilities $P_{(1975,\,NAT)}$, $P_{(1975,\,ALL)}$, and $P_{(2010,\,ALL)}$ are subsequently computed and are then used to compute the defined risk ratios. This process is repeated across the 500 × 474 reconstructions, leading to 500 × 474 estimates of each risk ratio. All estimates are used to derive the median and the 90% confidence intervals of the three defined risk ratios.

2.7. Observation-Constrained Projections

Assuming the fractional biases in the model responses stay constant over time (Allen et al., 2000), the estimates of scaling factors from the detection and attribution analyses may be used to produce observation-constrained projections of the future, that is the so-called ASK method. This assumption has

been found to be valid if external forcing increases linearly (Stott & Forest, 2007), and has been used to constrain projections of future air temperatures at global and regional scales (e.g., Allen et al., 2000; Stott & Kettleborough, 2002; Gillett et al., 2012; Mueller et al., 2016; Shiogama et al., 2016). We use this approach to produce observation-constrained projections of future summer WBGT under RCP8.5 for individual regions and for each of future decades from 2011–2020 to 2091–2100. We apply the ANT scaling factor from the 2-signal analysis to climate model simulated future changes in WBGT, rather than the ALL scaling factor of a 1-signal analysis which is used, for example, in Mueller et al. (2016), because the major scenario drivers of RCP8.5 are anthropogenic (Riahi et al., 2011). We transform the projected changes relative to 1973–2002 to absolute summer WBGT values by adding the observed 1973–2002 summer WBGT climatology to the projected changes. We use all data from all grid cells within a region to derive projections of the future. We are particularly interested in the timing when at least half of the projected summers have WBGT at least as large as the record WBGT.

It is noted that the ASK method also involves an implicit assumption that the relative contributions of different forcing components to the combined forcing (e.g., RCP8.5) remain constant over time. The RCP8.5 forcing scenario does not satisfy this assumption. Nevertheless, this should not be a serious limitation given that the historical ANT forcing and RCP8.5 forcing are dominated by anthropogenic emissions of greenhouse gases. An ASK method involving the individual responses of all forcing agents is expected to largely alleviate this problem (Shiogama et al., 2016). However, the necessary individual forcing simulations are not generally available from the CMIP5 climate models.

3. Results

3.1. Widespread Increases of Summer WBGT Are Occurring

Figure 1 shows trends in summer WBGT since 1973 in the observations and modeled responses to different forcings. Summer WBGT has increased over all land regions where there are sufficient data, with the most pronounced increases occurring in Europe and parts of North Asia (Figure 1a). This trend pattern is similar, in terms of both spatial distribution and magnitude, to that of summer air temperature (Figure S2a), suggesting that the widespread intensification of summer WBGT is largely a result of rising summer temperatures. This is consistent with Knutson and Ploshay (2016) who found that the global mean summer WBGT trend changes little if fixed climatological RH was used to compute WBGT. In fact, RH trend is small across the covered land (Figure S2b).

Widespread intensification of summer WBGT is also found in simulations when anthropogenic emissions of greenhouse gases are included as external forcing. The spatial pattern of the trends in ALL responses resembles that observed (Figure 1b). Although observed changes are larger than the modeled response to ALL in Europe and weaker than modeled in most other regions, the observed trends are within the range of trends computed from individual model runs. In fact, the observed trend lies within the central 90% of simulated trends in most grid cells (about 83% by area; Figure S3a). The GHG responses have a trend spatial pattern very similar to the ALL responses (Figure 1c), and capture the majority of the observed trends as well (about 69% by area; Figure S3b). Trends in the NAT responses, although positive, are very small (Figure 1e); the observed trends lie above the 95th percentile of trends computed from individual NAT runs in most grid cells (about 65% by area; Figure S3c). The OANT responses, which are estimated by subtracting the sum of modeled responses to GHG and NAT from ALL, exhibit an overall cooling pattern (Figure 1d).

The observed time series of continental mean summer WBGT is well within the range of simulations under ALL forcing, but it is above the range of simulations under NAT forcing (Figure 2b). Trends in the modeled responses to ALL and GHG are all positive and are of similar magnitudes to those observed. Trends in the modeled responses to NAT forcing are very weak. The OANT responses produce weakly negative trends in general (not shown). The negative OANT responses are not inconsistent with the relatively constant OANT forcing during the analyzed period as reported in Chapter 8 in IPCC WG1 (IPCC, 2013). Overall, it appears that the observed increases in summer WBGT can be reproduced by model simulations when GHG is included in external forcing but cannot be explained by NAT forcing alone.

3.2. Summer WBGT Increase Is Driven Primarily by Human Influence on the Climate

The influence of anthropogenic forcings (i.e., ANT, GHG, or OANT) is clearly detectable in the observed summer WBGT, but the influence of NAT is not detected (Figure 2c). This is consistent with Knutson and Ploshay

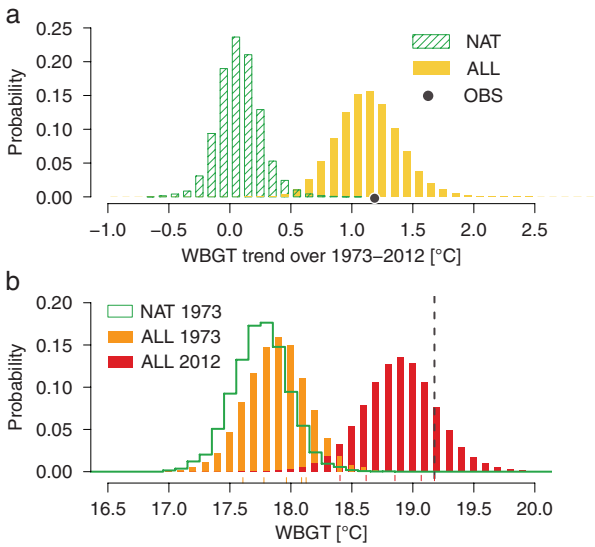

Figure 3. Anthropogenic influence has shifted summer wet bulb globe temperature (WBGT) toward higher levels. (a) Trend histograms of the observation-constrained 1973–2012 land average summer WBGT in a climate with (yellow) and without (green) anthropogenic influence. The observed trend is marked by a black point. (b) Histograms of the observation-constrained land average summer WBGT forced with only natural forcing in the climate around 1975 (represented by 1973–1977; green), with both natural and anthropogenic forcings in the climate forced around 1975 (orange) and around 2010 (represented by 2008–2012; red). The orange and red stick marks show the observations in the two periods, and the dashed vertical line shows the record land average summer WBGT experienced during 1973–2012, which occurred in 2010.

(2016). The best estimate of the scaling factor for ANT is slightly larger than one but the 90% uncertainty range of scaling factor includes one (pink bar in Figure 2c), suggesting that the modeled response to ANT may be somewhat underestimated but it is still consistent with the observations. The 90% confidence intervals for GHG and OANT scaling factors obtained from the three-signal analysis are both above one. As GHG and OANT are negatively correlated, an underestimation in the GHG response can be offset by a similar underestimation in OANT response. Thus, underestimation in both GHG and OANT may suggest a possible degeneration of the regression due to high correlation between the modeled responses (i.e., collinearity) and the difficulties in obtaining robust results when multiple correlated responses are involved in the detection analysis.

Of the observed 40-year warming of 1.08°C in land average summer mean WBGT, the amount that is attributable to anthropogenic forcing is estimated to be 1.04°C (90% confidence interval 0.63–1.47°C; pink bar in Figure 2d) based on the two-signal analysis. The observed warming in summer mean WBGT is smaller than the observed warming in summer mean air temperature of about 1.34°C based on HadISDH and 1.35°C based on CRUTEM4, consistent with the definition of indoor WBGT for which dry bulb temperature is an upper bound. From the three-signal analysis, we further find that increases of greenhouse gas alone could have induced a warming in summer mean WBGT of 1.55°C (1.04–2.25°C; purple bar in Figure 2d), and that this warming is offset by cooling from other anthropogenic forcings of 0.51°C (0.01–1.20°C; blue bar in Figure 2d). The net effect of warming in summer mean WBGT due to anthropogenic forcing is 1.04°C, consistent with the results from the two-signal analysis.

Both the two-signal and the three-signal analyses show consistently that the increase in summer WBGT is attributable to anthropogenic forcing but not to natural forcing. This is also reflected in a comparison between summer WBGT trends in the naturally forced world and in the world that is influenced by both natural and anthropogenic forcings (Figure 3a and Figure S4). Under natural forcing, the mean trend in land average summer WBGT is slightly positive but there is less than 1% chance for the NAT trend to be at least as large as that observed. On the other hand, the observed trend is close to the center of the trend distribution if anthropogenic forcing is also included. This result holds for individual SREX land regions as well (Figure S4).

Trends computed from observations and observation-constrained reconstructions under ANT for individual SREX regions show surprisingly good agreement (Figure 4a) despite the fact that the reconstructions are based on the results from a detection analysis that is conducted over all regions combined. This suggests that the observed intensification of regional summer WBGT is dictated largely by anthropogenic influence as well. A noticeable exception to this general observation occurs in the MED region, where the modeled responses to ANT forcing do not fully reproduce the observed warming. It has been suggested that this might be due to underestimation of the strength of soil–moisture–temperature feedbacks by climate models (van Oldenborgh et al., 2009), which has been found to play a crucial role in summer temperature variability in this region (Seneviratne et al., 2006). On the other hand, a regional discrepancy between

observed change and multi-model simulated change could also reflect the impact of internal variability in the observational record at the regional scale.

3.3. Human Influence Increases the Odds of the Record Summer WBGT

Anthropogenic influence up to the year 1973 had already significantly shifted the distribution of land average summer WBGT toward higher values relative to the world that might have been in the absence of anthropogenic influence (green versus orange histograms in Figure 3b). Following from further impact of changes in external forcing from 1973 to 2012, which is mainly anthropogenic in origin, the upper bound of land average summer WBGT in the climate around 1975 now represents roughly the median summer WBGT in the climate around 2010 (orange versus red histograms in Figure 3b). As a consequence, high heat stress summers are far more likely to occur in the present than in the past or in the naturally forced world. In particular, the record WBGT falls within the central 90% range of the distribution of summer WBGT in the actual climate around 2010, but would fall above the very end of the upper tail of the distribution in the climate around 1975 either with or without anthropogenic influence (black vertical line versus histograms in Figure 3b).

Conclusions based on the average summer WBGT over the entire land area are generally applicable to individual SREX regions. Figure 4b presents the defined risk ratios for the record WBGT RR_1, RR_2, and RR_3. We find that as of the year around 1975, anthropogenic influence had already made the record WBGT 2–13 times as likely across the regions (RR_1 shown by gray bars in Figure 4b) and that by the year around 2010 external forcing had further increased the regional risk ratios by factors ranging from about 30 in CNA to about 570 in MED (RR_2 shown by red bars in Figure 4b). Assuming a limited role of changes in natural forcing during 1973–2012, we estimate that by the year round 2010 the total impact of anthropogenic influence has made these record events about 70–1200 times as likely across the 10 SREX regions (RR_3 shown by yellow bars in Figure 4b). To put the results in perspective, consider as an example the record high summer mean WBGT in EAS, which occurred in 2010. We estimate that this would have been approximately a one-in-4300-year (90% confidence interval 2200–6100 years) event in the climate as it would have been at around 1975 under natural forcing only. Taking into account the combined effect of natural and anthropogenic forcing, we estimate that this was a one-in-890-year (420–1935 years) event in the actual climate around 1975 and it now occurs in this region on average once every 4 years (2–6 years).

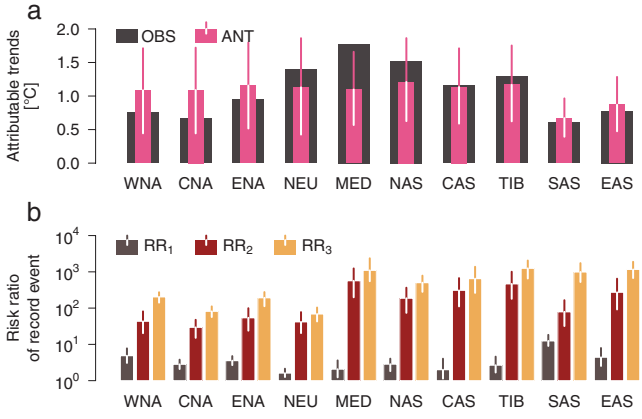

Figure 4. Anthropogenic influence dramatically increased the likelihood of record hot summer measured by wet bulb globe temperature (WBGT) during 1973–2012. (a) The observed trends (black bars), the best estimates (pink bars) and 5–95% ranges (whiskers) of the trends attributable to anthropogenic influence in summer (Jun-Jul-Aug) WBGT in the 10 SREX regions. (b) The best estimates (bars) and 5–95% ranges (whiskers) of risk ratios of the record summer WBGT experienced during 1973–2012 in the 10 SREX regions. RR_1, RR_2, and RR_3 denote respectively to ratios of the probability of the record summer mean regional WBGT in the climate around 1975 (represented by 1973–1977) forced with both natural and anthropogenic forcings compared to that forced with only natural foricng, the probability in the climate around 2010 (represented by 2008–2012) compared to that around 1975 forced with both natural and anthropogenic forcings, and the probability in the climate around 2010 forced with both natural and anthropogenic forcings compared to that in the climate around 1975 forced with only natural forcing.

These results are broadly consistent with those reported by Christidis et al. (2012), Sun et al. (2014), and Meuller et al. (2016) on changes in the likelihood of historically highest summer TA due to anthropogenic influence. A key difference, however, is that impact of anthropogenic influence on the relative likelihood of extreme WBGT appears to be about an order of magnitude greater than that on TA. Specifically, we find that the risk ratios for the record summer TA are smaller than those for the record summer WBGT if all other conditions such as the spatial and temporal coverage of data are equal (orange versus blue bars Figure 5).

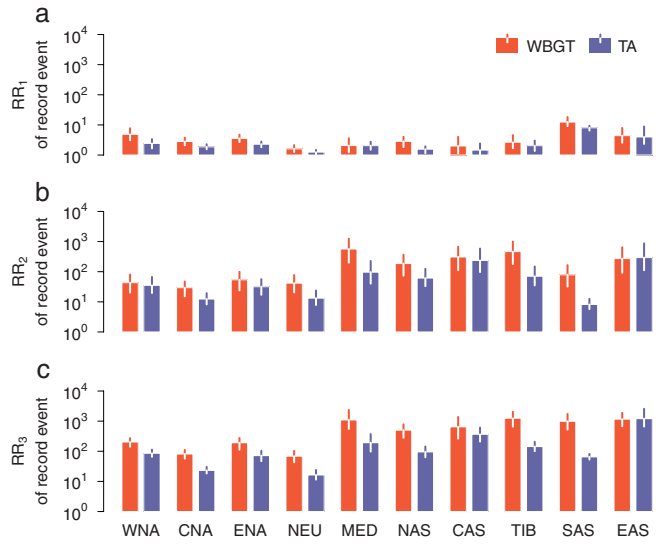

Figure 5. For the record hot summers indicated respectively by summer (Jun–Jul–Aug) wet bulb globe temperature (WBGT) and air temperature (TA), the risk ratios are larger for WBGT than TA. Panels show the best estimates (bars) and 5–95% uncertainty ranges (whiskers) of RR_1 (a), RR_2 (b), and RR_3 (c) of the record summer WBGT (orange) and TA (blue) during 1973–2012 in the 10 SREX regions. Definitions for RR_1, RR_2, and RR_3 are the same as in Figure 4.

Statistically, this occurs mainly because WBGT has smaller variability when compared with TA (Figure S5). For the record heat summers indicated respectively by summer mean WBGT and TA, RR_3 is larger for WBGT than for TA by a factor of about 3–15 in all the analyzed regions except EAS (orange versus blue bars in Figure 5 bottom panel), with the difference exceeding uncertainty in most cases. Given the relevance of WBGT as an indicator of potential human heat stress and a tool for its management, this is of significant concern, particularly for regions with hot and humid climates, such as SAS. Even in regions where there is a drying trend in relative humidity such as MED and EAS (Figure S2 bottom panel), where we would expect reductions in relative humidity to offset some of the impact of warming on environmental conditions conducive to heat stress, our results suggest that the increase in potential evaporation is not sufficient to prevent an increase in the likelihood of environmental conditions conducive to heat stress (with summer WBGT exceeding historical records during 1973–2012).

3.4. The Record Summer WBGT will Become the Norm within 20 years

The warming due to human influence is projected to continue in the future, resulting in more severe and more frequent summers with high WBGT values. The observation-constrained projections under the RCP8.5 scenario estimate the median summer WBGT (red points in Figure 6) to be higher than the historically highest values in all SREX regions no later than the 2030s, which would make the record WBGT the new norm within 20 years. In WNA, TIB, and EAS, this new reality appears to be emerging in the present decade, and in half of the regions (CNA, ENA, MED, NAS, and EAS) it may emerge as early as the decade of 2020s. By the middle of the 21st century, WBGT is projected to exceed its historical record in more than 95% of summers (horizontal lines versus shaded envelopes in Figure 6). These results are also consistent with earlier projections (Christidis et al., 2014; Mueller et al., 2016; Sun et al., 2014) on the hottest summer TA under the same emissions scenario. For instance, Sun et al. (2014) projected that by 2022, at least half of all summers will be as hot as the 2013 summer in Eastern China; Christidis et al. (2014) projected that by the 2030s a summer as hot as 2003 in Europe will be very common; Mueller et al. (2016) found that in many northern hemispheric land regions the hottest summers during 1951–2012 will be a new norm within a decade and a 9-in-10-year event by the 2040s.

Although we focus this study on the RCP8.5 scenario, given that the projected future temperature increase does not significantly diverge under different RCP scenarios until 2030 (IPCC AR5 SPM, 2013), the reported projections indicate an apparently unavoidable reality in the very near future of substantial intensification of environmental conditions conducive to increased heat stress, adding to the need for rapid development of adaptation measures (Zhang et al., 2008).

4. Conclusions and Discussion

In this study, we examined trends in summer mean WBGT since 1973. We compared observed summer mean WBGT with model simulated responses to different external forcings. We found that summer mean

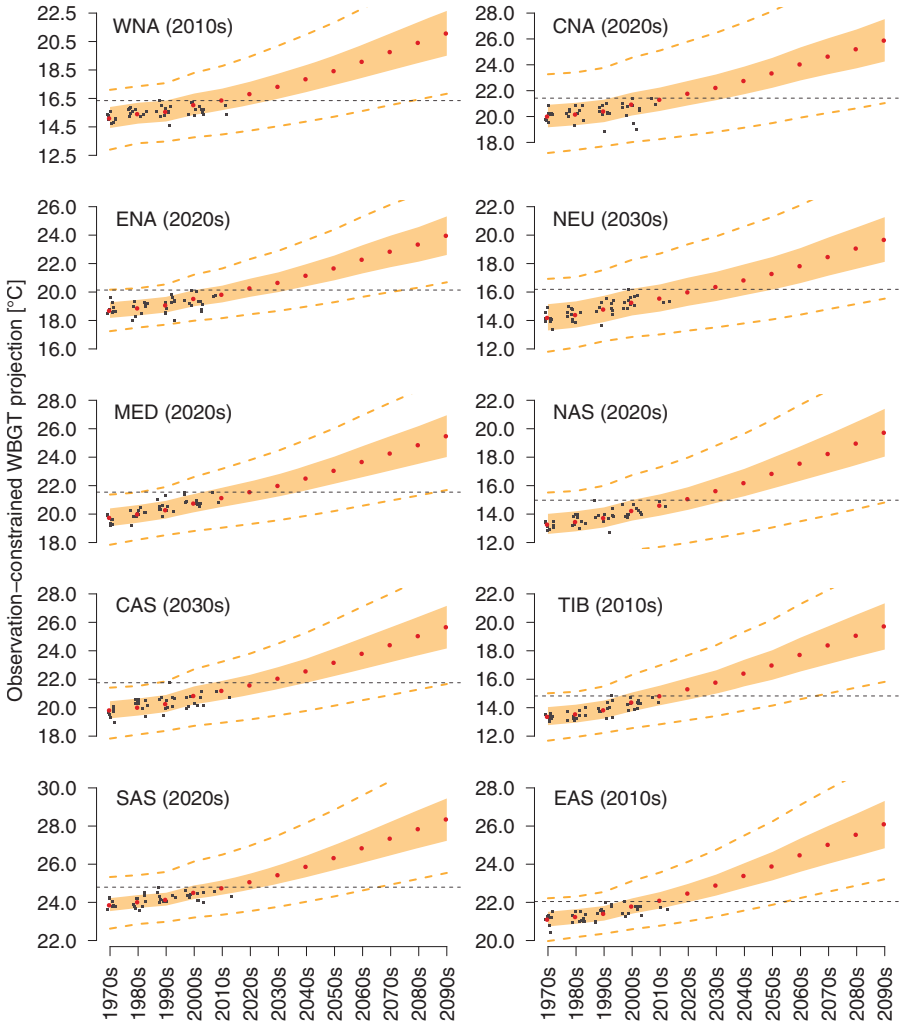

Figure 6. Record hot summers during 1973–2012 measured by wet bulb globe temperature (WBGT) are likely to be the future norm within 20 years in all regions. Panels show the observation-constrained projections of future summer (Jun–Jul–Aug) wet bulb globe temperature under the representative concentration pathway emissions scenario RCP8.5 in the 10 SREX regions. The red points, yellow envelopes, and dashed curves represent the medians, 5–95% ranges, and full ranges of the constrained projections. Summer WBGT observations are shown by black points, with the highest ones marked by dashed horizontal lines. Numbers in parentheses show the decades when half of the projected summers will have WBGT at least as large as the record WBGT experienced during 1973–2012.

WBGT has increased over land areas and that these changes cannot be explained by internal climate variability, nor by natural external forcing alone. Only with the inclusion of anthropogenic forcing can the observed changes be explained. We found that of the observed 1973–2012 summer mean WBGT warming of 1.08°C, greenhouse gas increases alone could have caused a warming of 1.55°C (90% confidence interval 1.04–2.25°C), which may have been partially offset by 0.51°C (0.01–1.20°C) due to the cooling effect from other anthropogenic forcings including aerosols, ozone and land use change. We also found that the total impact of anthropogenic influence may have made the historically highest summer WBGT since 1973 at least 70 times as likely relative to the naturally forced world. We further estimate that, in most regions, these anthropogenically induced changes in the likelihood of extreme summer mean WBGT are roughly an order of magnitude larger than the corresponding changes in the likelihood of extreme warm summers as simply measured by surface air temperature, due to the relatively lower variance of summer mean WBGT. Although a decrease in relative humidity has been found in many land regions (Willett et al., 2014), the increase in potential evaporation is not sufficient to prevent an increase in the likelihood of summers with WBGT exceeding historical records during 1973–2012. Based on the detection and attribution analysis as well as model simulated future changes in WBGT under the RCP8.5 scenario, we projected that by the 2030s,

more than 50% summers will have WBGT higher than the historical record, and that this percentage will increase to 95% by the middle of the 21st century.

Climate models may have considerable biases in simulating RH (Dunn et al., 2017), which could potentially undermine the reliability of detection and attribution analyses of RH-related variables. Nevertheless, our study shows that the observed WBGT trend is well within the range of modeled WBGT trend across the land area with adequate observations. There is also evidence from formal detection and attribution analyses that the observed changes in summer WBGT are indeed consistent with model simulated responses to external forcing. These suggest that results based on model simulated changes in WBGT should be sufficiently robust.

In our study, we computed WBGT based on monthly values of TA and RH. As WBGT is not a linear function of TA and RH, especially in hot regions with high RH (Stull, 2011), monthly values of WBGT calculated from monthly mean TA and RH can be different from that calculated based on daily data. Based on the WATCH-Forcing-Data-ERA-Interim reanalysis data over 1979–2014 (Weedon et al., 2014), we found only a small difference between summer WBGT estimates that are computed from monthly or daily values at the scales considered in this study.

Acknowledgments

We thank Daithi Stone for helpful comments on the manuscript. We thank the Program for Climate Model Diagnosis and Intercomparison and the World Climate Research Programme's Working Group on Coupled Modeling for making the WCRP CMIP multi-model data set available (https://www.wcrp-climate.org/wgcm-cmip). We acknowledge the UK Met Office for access to the HadISDH observational data (http://www.metoffice.gov.uk/hadobs/hadisdh/). C.L. and A.M. acknowledge funding from National Science Foundation under grant agreement no.1313897. This study was partly conducted at Carnegie Intuition for Science at Stanford University when C.L. worked there as a Barbara McClintock Postdoctoral Fellow in A.M.'s group.

References

Allen, M. R., Scott, P. A., Mitchell, J. F. B., Schnur, R., & Delworth, T. L. (2000). Quantifying the uncertainty in forecasts of anthropogenic climate change. *Nature*, *407*, 617–620. https://doi.org/10.1038/35036559

Allen, M. R., & Stott, P. A. (2003). Estimating signal amplitudes in optimal fingerprinting: I. Theory. *Climate Dynamics*, *21*, 477–491. https://doi.org/10.1007/s00382-003-0313-9

Buzan, J. R., Oleson, K., & Huber, M. (2015). Implementation and comparison of a suite of heat stress metrics within the Community Land Model version 4.5. *Geoscientific Model Development*, *8*, 151–170. https://doi.org/10.5194/gmd-8-151-2015

Christidis, N., Jones, G. S., & Stott, P. A. (2014). Dramatically increasing chance of extremely hot summers since the 2003 European heatwave. *Nature Climate Change*, *5*, 46–50. https://doi.org/10.1038/nclimate2468

Christidis, N., Stott, P. A., Zwiers, F. W., Shiogama, H., & Nozawa, T. (2010). Probabilistic estimates of recent changes in temperature: A multi-scale attribution analysis. *Climate Dynamics*, *34*, 1139–1156. https://doi.org/10.1007/s00382-009-0615-7

Christidis, N., Stott, P. A., Zwiers, F. W., Shiogama, H., & Nozawa, T. (2012). The contribution of anthropogenic forcings to regional changes in temperature during the last decade. *Climate Dynamics*, *39*, 1259–1274. https://doi.org/10.1007/s00382-011-1184-0

Diffenabugh, N. S., Pal, J. S., Giorgi, F., & Gao, X. (2007). Heat stress intensification in the Mediterranean climate change hotspot. *Geophysical Research Letters*, *34*, L11706. https://doi.org/10.1029/2007GL030000

Dunn, R. J. H., Willet, K. M., Ciavarella, A., & Stott, P. A. (2017). Comparison of land-surface humidity between observations and CMIP5 models. *Earth System Dynamics: Discussion*, 1–36. https://doi.org/10.5194/esd-2017-9

Dunne, J. P., Stouffer, R. J., & John, J. G. (2013). Reductions in labour capacity from heat stress under climate warming. *Nature Climate Change*, *3*, 563–566.

Fisher, E. M., & Knutti, R. (2012). Robust projections of combined humidity and temperature extremes. *Nature Climate Change*, *3*, 126–130. https://doi.org/10.1038/nclimate1682

Gillett, N. P., Flato, G. M., Scinocca, J. F., & von Salzen, K. (2012). Improved constraints on 21st-century warming derived using 160 years of temperature observations. *Geophysical Research Letters*, *37*, L01704. https://doi.org/10.1029/2011GL050226

Intergovernmental Panel on Climate Change (IPCC) (2013). In T. Stocker, et al. (Eds.), *The physical science basis Contribution of Working Group I to the Fifth Assessment Report of the Intergovernmental Panel on Climate Change* (). Cambridge, England: Cambridge University Press.

International Standards Organization (ISO) (1989). Hot Environments—Estimation of the heat stress on working man, based on the WBGT-index (wet bulb globe temperature), *ISO Standard 7243* (). Geneva: International Standards Organization.

Knutson, T. R., & Ploshay, J. J. (2016). Detection of anthropogenic influence on a summertime heat stress index. *Climatic Change*, *138*, 25–39. https://doi.org/10.1007/s10584-016-1708-z

Lemke, B., & Kjellstrom, T. (2012). Calculating workplace WBGT from meteorological data: A tool for climate change assessment. *Industrial Health*, *50*, 267–278. https://doi.org/10.2486/indhealth.MS1352

Liljegren, J. C., Carhart, R. A., Lawday, P., Tschopp, S., & Sharp, R. (2008). Modeling the wet bulb globe temperature using standard meteorological measurements. *Journal of Occupational and Environmental Hygiene*, *5*, 645–655. https://doi.org/10.1080/15459620802310770

Mueller, B., Zhang, X., & Zwiers, F. W. (2016). Historically hottest summers projected to be the norm for more than half of the world's population within 20 years. *Environmental Research Letters*, *11*, 044011. https://doi.org/10.1088/1748-9326/11/4/044011

Pal, J. S., & Eltahir, E. A. B. (2015). Future temperature in southwest Asia projected to exceed a threshold for human adaptability. *Nature Climate Change*, *6*, 197–200.

Parsons, K. (2003). Human thermal environments. In *The effects of hot, moderate and cold temperatures on human health, comfort and performance* (2nd ed.). London: Taylor & Francis.

Riahi, K., Rao, S., Krey, V., Cho, C., Chirkov, V., Fischer, G., Kindermann, G., Nakicenovic, N., & Rafaj, P. (2011). RCP8.5—A scenario of comparatively high greenhouse gas emissions. *Climatic Change*, *109*, 33–57. https://doi.org/10.1007/s10584-011-0149-y

Ribes, A., Planton, S., & Terray, L. (2013). Application of regularised optimal fingerprinting to attribution. Part I: Method, properties and idealised analysis. *Climate Dynamics*, *4*, 2817–2836.

Sen, P. K. (1968). Estimates of the regression coefficient based on Kendall's tau. *Journal of the American Statistical Association*, *63*, 1379–1389. https://doi.org/10.1080/01621459.1968.10480934

Seneviratne, S., Lüthi, D., Litschi, M., & Schär, C. (2006). Land-atmosphere coupling and climate change in Europe. *Nature*, *443*, 205–209. https://doi.org/10.1038/nature05095

Seneviratne, S., Nicholls, N., Easterling, D., Goodess, C. M., Kanae, S., Kossin, J., … Zhang, X. (2012). In C. B. Field, et al. (Eds.), *Managing the risks of extreme events and disasters to advance climate change adaptation. A special Report of Working Groups I and II of the Intergovernmental Panel on Climate Change* (pp. 109–230). Cambridge, England: Cambridge University Press.

Sherwood, S. C., & Huber, M. (2010). An adaptability limit to climate change due to heat stress. *Proceedings of the National Academy of Sciences of the United States of America*, *107*, 9552–9555. https://doi.org/10.1073/pnas.0913352107

Shiogama, H., Stone, D., Emori, S., Takahashi, K., Mori, S., Maeda, A., Ishizaki, Y., & Allen, M. R. (2016). Predicting future uncertainty constraints on global warming projections. *Scientific Reports*, *6*, 18903. https://doi.org/10.1038/srep18903

Stott, P. A., & Forest, C. E. (2007). Ensemble climate predictions using climate models and observational constraints. *Philosophical Transactions of the Royal Society of London A*, *365*, 2029–2052. https://doi.org/10.1098/rsta.2007.2075

Stott, P. A., & Kettleborough, J. A. (2002). Origins and estimates of uncertainty in predictions of twenty-first century temperature rise. *Nature*, *416*, 723–726. https://doi.org/10.1038/416723a

Stott, P. A., Stone, D. A., & Allen, M. R. (2004). Human contribution to the European heatwave of 2003. *Nature*, *432*, 610–613. https://doi.org/10.1038/nature03089

Stull, R. (2011). Wet-bulb temperature from relative humidity and air temperature. *Journal of Applied Meteorology and Climatology*, *50*, 2267–2269. https://doi.org/10.1175/JAMC-D-11-0143.1

Sun, Y., Zhang, X., Zwiers, F. W., Song, L., Wan, H., Hu, T., Yin, H., & Ren, G. (2014). Rapid increase in the risk of extreme summer heat in eastern China. *Nature Climate Change*, *4*, 1082–1085. https://doi.org/10.1038/nclimate2410

van Oldenborgh, G. J., Drijfhout, S., van Ulden, A., Haarsma, R., Sterl, S., Severijns, C., Hazeleger, W., & Dijkstra, H. (2009). Western Europe is warming much faster than expected. *Climate of the Past*, *5*, 1–12. https://doi.org/10.5194/cp-5-1-2009

Weedon, G. P., Balsamo, G., Bellouin, N., Gomes, S., Best, M. J., & Viterbo, P. (2014). The WFDEI meteorological forcing data set: WATCH forcing data methodology applied to ERA-interim reanalysis data. *Water Resources Research*, *50*, 7505–7514. https://doi.org/10.1002/2014WR015638

Willet, K. M., & Sherwood, S. C. (2012). Exceedance of heat index thresholds for 15 regions under a warming climate using the wet-bulb globe temperature. *International Journal of Climatology*, *32*, 161–177. https://doi.org/10.1002/jocjoc.2257.

Willett, K. M., Dunn, R. J. H., Thorne, P. W., Bell, S., de Podesta, M., Parker, D. E., Jones, P. D., & Williams Jr., C. N. (2014). HadISDH land surface multi-variable humidity and temperature record for climate monitoring. *Climate of the Past*, *10*, 1983–2006. https://doi.org/10.5194/cp-10-1983-2014

Zhang, X., Zwiers, F. W., & Peterson, T. C. (2008). The adaptation imperative: Is climate science ready? *WMO Bulletin*, *57*(2).

Zhao, Y., Ducharne, A., Sultan, B., Braconnot, P., & Vautard, R. (2015). Estimating heat stress from climate-based indicators: Present-day biases and future spreads in the CMIP5 global climate model ensemble. *Environmental Research Letters*, *10*, 084013. https://doi.org/10.1088/1748-9326/10/8/084013